LANGMUIR

Article

pubs.acs.org/Langmuir

# Comparative Study of the Oxidation of NiAl(100) by Molecular Oxygen and Water Vapor Using Ambient-Pressure X-ray Photoelectron Spectroscopy

Qianqian Liu,[†] Hailang Qin,[†] Jorge Anibal Boscoboinik,[‡] and Guangwen Zhou*[,†]

[†]Department of Mechanical Engineering & Multidisciplinary Program in Materials Science and Engineering, State University of New York, Binghamton, New York 13902, United States

[‡]Center for Functional Nanomaterials, Brookhaven National Laboratory, Upton, New York 11973, United States

**ABSTRACT:** The oxidation behavior of NiAl(100) by molecular oxygen and water vapor under a near-ambient pressure of 0.2 Torr is monitored using ambient-pressure X-ray photoelectron spectroscopy. $O_2$ exposure leads to the selective oxidation of Al at temperatures ranging from 40 to 500 °C. By contrast, $H_2O$ exposure results in the selective oxidation of Al at 40 and 200 °C, and increasing the oxidation temperature above 300 °C leads to simultaneous formation of both Al and Ni oxides. These results demonstrate that the $O_2$ oxidation forms a nearly stoichiometric $Al_2O_3$ structure that provides improved protection to the metallic substrate by barring the outward diffusion of metals. By contrast, the $H_2O$ oxidation results in the formation of a defective oxide layer that allows outward diffusion of Ni at elevated temperatures for simultaneous NiO formation.

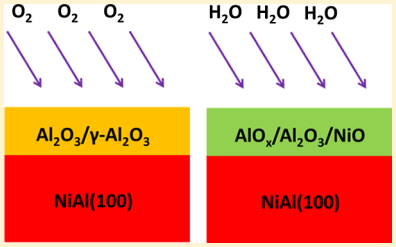


## 1. INTRODUCTION

NiAl is a technologically important intermetallic material possessing a high melting point, low density, good oxidation/corrosion resistance, and metal-like electrical and thermal conductivities. Thin aluminum oxide films grown by selective oxidation of Al in the NiAl alloy are widely used as one of the most important supports for dispersed metal catalysts.[1−5] Because of this important industrial application and also the fundamental importance in understanding the degradation mechanism of intermetallic alloys, the initial-stage oxidation of single-crystal NiAl(100) has been extensively studied to address the atomistic mechanism of the formation of ultrathin aluminum oxide films using a wide range of surface science tools including low-energy electron diffraction (LEED),[6−11] X-ray photoelectron spectroscopy (XPS),[11−13] electron energy loss spectroscopy,[6,7] scanning tunneling microscopy (STM),[8−11,14−16] and low-energy electron microscopy (LEEM).[10,16] These surface science studies of the oxidation of NiAl are performed mostly under ultrahigh vacuum (UHV) conditions by carefully dosing small amounts of oxygen gas. Although the surface science approach has been very successful in many cases as shown in the aforementioned studies, the pressure gap between the surface science experiments and the technologically relevant oxidation processes that often take place within high-temperature and high-pressure regimes prevents the direct extrapolation of the knowledge obtained from the idealized condition. This is because the structure and composition of the surface can drastically change when going from UHV to realistic situations. Therefore, the effects of temperature and pressure must be properly accounted for to obtain a reliable description of the surface structure/chemistry and transformations under the technologically relevant conditions.

Recent advances in instrumentation have made it possible to investigate gas−surface reactions under realistic pressures with in situ measurements. Particularly, XPS has evolved dramatically in recent years with the implementation of differential pumping schemes that allow for the investigation of surface reactions on the atomic scale at a gas pressure of up to ∼1 Torr.[17−21] Because the formation of an oxide layer on the metal surface is expected to dramatically change its chemical properties, using these in situ techniques for oxidation studies will provide unique opportunities to establish the principles of controlling the atomic processes of surface oxidation via manipulating the thermodynamic and kinetic variables of the reaction including temperature, oxygen pressure, surface orientation and morphology, and alloying.

Under ambient conditions, the reaction of NiAl with oxygen or an oxygen-containing atmosphere such as water vapor results in selective oxidation of Al. The reaction proceeds with the initially rapid growth of a thin layer of aluminum oxide followed by an abrupt reduction in the oxidation rate, thereby reaching a limiting thickness of the oxide film. Compared with the extensive study on the oxidation of a clean metal surface, the lack of a fundamental understanding of the effect of such a passivation oxide layer on the subsequent oxidation at elevated temperatures has not been addressed. In this work, we report an in situ study of the oxidation of NiAl(100) in a more practical oxidation condition, namely an ambient gas pressure, using ambient pressure X-ray photoelectron spectroscopy (AP-XPS). We perform a comparative study of the oxidation of NiAl(100) with molecular oxygen and water vapor at the near-

**Received:** July 25, 2016
**Revised:** October 4, 2016
**Published:** October 11, 2016





DOI: 10.1021/acs.langmuir.6b02752
*Langmuir* 2016, 32, 11414−11421

ambient pressure of 0.2 Torr, with a stepwise increase in temperature from 40 to 500 °C. With the temperature increase in such a stepwise manner, our experiments here allow for examining the oxidation behavior of a surface covered with a pre-existing oxide film that forms at a lower temperature and resembles the presence of a native oxide layer. The use of molecular oxygen and water vapor as the oxidizing species allows for elucidating how the growth and properties of the oxide film depend on the oxidizing atmosphere, which has been rarely addressed at the atomic scale under such a high pressure.

## 2. EXPERIMENTAL

AP-XPS experiments were performed in an AP-XPS chamber equipped with a SPECS Phoibos 150 analyzer and an Ar-ion-sputtering gun at beamline X1A1 at the National Synchrotron Light Source (NSLS), Brookhaven National Laboratory. The AP-XPS system is equipped with several differential pumping stages between the reaction chamber and the hemispherical analyzer, which results in different gas pressures in these two chambers, that is, up to several Torr in the reaction chamber but remaining under ultrahigh vacuum conditions (lower than $10^{-7}$ Torr) in the analyzer. Photoemitted electrons leave the high-pressure chamber through a small aperture into the multistage differentially pumped electron energy analyzer that allows for continuous collection of XPS signals from the sample enclosed in the elevated pressure volume. The XPS spectra of the gas phases ($O_2$ and $H_2O$) can be observed at pressures >0.1 Torr. The photon energy range of the beamline was from ~200 to ~850 eV, which covers the O 1s, C 1s, Al 2p, and Ni 3p core levels. An Au foil in the XPS chamber was used to calibrate the real incident photon energy for acquiring XPS data. In the $O_2$ oxidation experiment, the real incident photon energy was 707 eV. The $H_2O$ oxidation experiment was performed a few months later, and the real incident photon energy was 683 eV because of the change in the positions of the motors that drove the monochromator. Spectra of Ni 3p, Al 2p, and O 1s were acquired in situ during the oxidation.

The NiAl(100) single crystal purchased from Princeton Scientific Corp was a top-hat-shaped disc (1 mm in thickness and 8 mm in diameter) and cut to within 0.1° to the (100) crystallographic orientation and polished to a mirror finish with a purity of 99.9999%. The NiAl(100) crystal was cleaned by repeated cycles of Ar-ion sputtering ($1 \times 10^{-5}$ Torr, 1 keV) at room temperature and annealing at 750 °C for about 10 min, until no carbon was detected using XPS. However, a small amount of oxygen was still present as detected in O 1s XPS spectra and could not be completely removed, likely due to the relatively high base pressure of the XPS chamber (the presence of such residual oxygen had negligible impact on the oxidation experiments performed under near-ambient conditions). The sample temperature was measured using a K-type thermocouple. A separate system equipped with the capabilities for surface structure characterization, that is, LEED and STM, was used to check the surface quality of the NiAl(100) prepared using the same sputtering and annealing procedure as the AP-XPS experiments. The as-cleaned surface showed sharp diffraction spots of the $c(3\sqrt{2} \times 3\sqrt{2}, \sqrt{2} \times 3\sqrt{2})R45°$ reconstruction[15,22] and appeared as flat terraces separated by atomic height steps.

High-purity oxygen gas was directly introduced to the XPS chamber through a variable-pressure leak valve to oxidize the freshly cleaned NiAl(100). Water (18.2 MΩ) was poured into a glass flask (Ace Glass) and further purified with several freeze–pump–thaw cycles before dosing through a separate variable-pressure leak valve. Ion gauges were used to measure the gas pressures. The effect of the ion gauge sensitivity correction was not accounted for during the pressure measurements because of the minor difference in the gas correction factors for $O_2$ and $H_2O$. No carbon contamination was detected using XPS from the $O_2$ and $H_2O$ exposures. The freshly cleaned surface was exposed to $O_2$ or $H_2O$ at the pressure of 0.2 Torr first at $T$ = 40 °C, followed by the stepwise temperature increase to 200, 300, and 500 °C during the gas exposure. Under each condition, the surface was oxidized to a saturated thickness of the oxide film, unless noted otherwise. After the oxidation at 500 °C, the chamber was evacuated and the sample was annealed at 500 and 750 °C in vacuum to investigate the temperature effect on the atomic structure of the oxide film. The conditions for oxidation and subsequent vacuum annealing are detailed in Table 1.

**Table 1. Conditions for the $O_2$ and $H_2O$ Oxidation of NiAl(100) and Subsequent Annealing of the Oxide Film**

| temperature (°C) | 40 | 200 | 300 | 500 | 500 vacuum annealing | 750 vacuum annealing |
|---|---|---|---|---|---|---|
| $O_2$ (min) | 30 | 30 | 30 | 30 | 30 | 30 |
| $H_2O$ (min) | 25 | 20 | 30 | 40 | 20 | 20 |

At each temperature during the gas exposure and annealing, the XPS spectra of O 1s, Ni 3p, and Al 2p were acquired at 10, 20, and 30 min or longer as required. Each spectrum was fitted with a Shirley background subtraction. The binding energy (BE) extracted was estimated to have an error of less than 0.05 eV. The thickness of the oxide film was calculated using the ratio of the total oxidic $Al^{3+}$ 2p and the metallic $Al^0$ 2p peak areas in each single XPS spectrum of the oxidized NiAl(100) surface, assuming a uniform oxide layer, and was estimated to have an error of less than 1–2 Å.[22,23] The inelastic mean free path $\lambda$ was estimated by the kinetic energy of Al 2p that depends on the incident photon energies. In the $O_2$ oxidation experiments, $\lambda \approx$ 11.3 Å for the incident photon energy of 707 eV; in the $H_2O$ oxidation experiments, $\lambda \approx$ 10.8 Å for the incident photon energy of 683 eV.[24] This indicates that the small difference in the incident photon energies (24 eV) used in acquiring the XPS data during the $O_2$ and $H_2O$ oxidations has a negligible effect on the detectable oxide thicknesses (less than 1 Å). The BE scale was calibrated by measuring Fermi edge spectra of Ni. The peak intensities were normalized by the highest intensity value in each spectrum. The intensities of the spectra between different oxidation temperatures were not compared because the photoelectron counts can be affected by gas-phase molecules.[17]

## 3. RESULTS

**3.1. Oxidation by Molecular Oxygen.** The freshly cleaned NiAl(100) surface was first oxidized by oxygen gas at $p(O_2)$ = 0.2 Torr and at temperatures ranging from $T$ = 40 to 500 °C. Figure 1a,b shows the evolution of the XPS spectra of the O 1s and Al 2p/Ni 3p regions during the oxidation under the conditions given in Table 1. The oxide film reached its limiting thickness after the $O_2$ exposure at each $T$. As seen in Figure 1a, the O 1s region shows a very low intensity peak for the freshly cleaned NiAl(100) surface, which can be attributed to the residual oxygen that cannot be completely removed by sputtering and annealing because of the relatively high base pressure (~$7 \times 10^{-9}$ Torr) of the chamber. This can also be proved by the small intensity of the $Al^{3+}$ 2p peak in the corresponding Al 2p spectrum obtained from the freshly cleaned NiAl(100) surface (Figure 1b). After exposure to $p(O_2)$ = 0.2 Torr with the stepwise temperature increase from 40 to 500 °C and the holding time of 30 min for each $T$, the O 1s spectra show a clear trend of increase in the BE.

Figure 1b shows the corresponding XPS spectra in the Al 2p/Ni 3p regions. It can be seen that the BEs of the metallic $Ni^0$ 3p and $Al^0$ 2p peaks do not show any noticeable shift with the temperature increase. However, the BE of the $Al^{3+}$ 2p peak shows a clear shift to a higher value. This is also qualitatively consistent with the studies on the thermal oxidation of aluminum[25] and our earlier results on NiAl(100) under the UHV conditions of $O_2$ exposure.[13] Also, it is worthwhile to note that the intensities of the metallic $Ni^0$ 3p and $Al^0$ 2p peaks diminish and disappear completely at 500 °C, whereas the peak



DOI: 10.1021/acs.langmuir.6b02752
Langmuir 2016, 32, 11414–11421

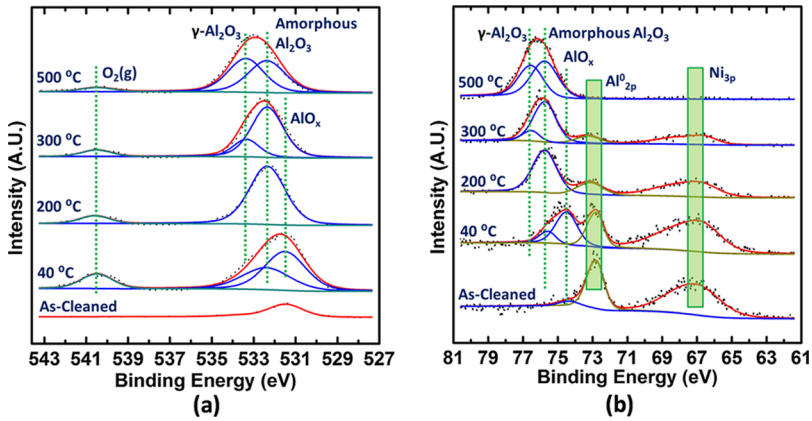


**Figure 1.** Photoemission spectra of the O 1s (a) and Al 2p−Ni 3p (b) regions of the NiAl(100) during the stepwise $O_2$ oxidation at $p(O_2)$ = 0.2 Torr and at $T$ = 40, 200, 300, and 500 °C. Oxidation time is 30 min at each $T$.

**Table 2. Comparison of the Binding Energies of O 1s for the $O_2$- and $H_2O$-Formed Oxide Films**

| | O 1s | | | | | | | | | |
|---|---|---|---|---|---|---|---|---|---|---|
| | $AlO_x$ | | amorphous $Al_2O_3$ | | $\gamma$-$Al_2O_3$ | | Al-OH | | NiO | |
| | $O_2$ (eV) | $H_2O$ (eV) | $O_2$ (eV) | $H_2O$ (eV) | $O_2$ (eV) | $H_2O$ (eV) | $O_2$ (eV) | $H_2O$ (eV) | $O_2$ (eV) | $H_2O$ (eV) |
| 40 °C | 531.3 | 531.3 | 532.4 | 532.4 | | | | 533.8 | | |
| 200 °C | | 531.3 | 532.4 | 532.4 | | | | 533.8 | | |
| 300 °C | | 531.3 | 532.4 | 532.4 | 533.3 | | | | | 530.3 |
| 500 °C | | 531.3 | 532.4 | 532.4 | 533.3 | | | | | 530.3 |
| 500 °C vacuum annealing | | 531.3 | 532.4 | 532.4 | 533.3 | | | | | 530.3 |
| 750 °C vacuum annealing | | 531.3 | 532.4 | 532.4 | 533.3 | 533.3 | | | | 530.3 |

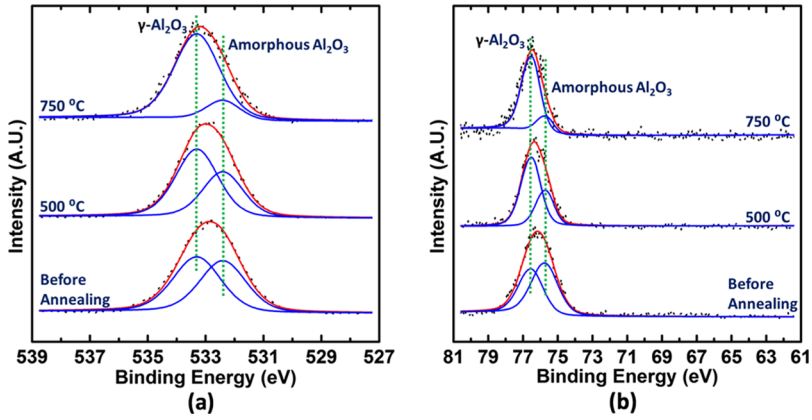


**Figure 2.** Photoemission spectra of the (a) O 1s and (b) Al 2p−Ni 3p regions of the NiAl(100) during the stepwise $O_2$ oxidation at $p(O_2)$ = 0.2 Torr and subsequent annealing at 500 °C and then at 750 °C for 30 min each. The spectra for vacuum annealing were taken in vacuum at the corresponding annealing temperatures.

intensity of the $Al^{3+}$ 2p peak is very strong, indicating that the oxide film has reached a certain thickness at which the metallic peaks are completely attenuated. The oxide film shows stepwise increase in its thickness with the stepwise increase in the temperature and reaches about 22 Å after the $O_2$ exposure at 300 °C, as shown in Table 2. The thickness after oxidation at 500 °C is even larger but is not estimated here because the metallic $Al^0$ 2p peak is completely attenuated.

As can be seen in Figure 1a, the O 1s peak from the $O_2$ exposure at 40 °C is well fit by two components at BE = 532.4 and 531.3 eV. The 532.4 eV component is in good agreement with the reported values of O in amorphous $Al_2O_3$,[20,26,27] whereas the lower BE at 531.3 eV is attributed to O from the interfacial aluminum oxide, which can be designated Al-deficient $AlO_x$.[20,27,28] As seen in Figure 1a, the oxide consists of mainly $AlO_x$ and a small amount of $Al_2O_3$ after the $O_2$ exposure at 40 °C. However, the peak corresponding to $AlO_x$ at BE = 531.3 eV disappears after the oxidation at 200 °C, indicating that the $AlO_x$ component is completely converted to the more stoichiometric $Al_2O_3$ component. After the $O_2$ exposure at $T$ = 300 °C, another peak at a higher BE of 533.3 eV arises. This peak is assigned to the O in the crystalline $Al_2O_3$ ($\gamma$-$Al_2O_3$), which is 0.9 eV higher than the BE of the amorphous $Al_2O_3$ and in good agreement with the reported difference (0.5−1.0 eV) between the amorphous $Al_2O_3$ and $\gamma$-$Al_2O_3$.[25,29] When the temperature is further increased to 500 °C, the amount of amorphous $Al_2O_3$ component decreases, whereas the amount of $\gamma$-$Al_2O_3$ increases, indicating that more



DOI: 10.1021/acs.langmuir.6b02752
Langmuir 2016, 32, 11414−11421

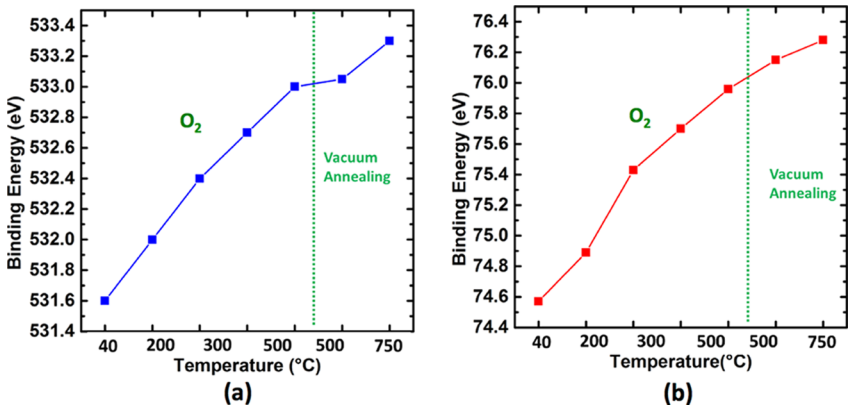


**Figure 3.** Evolution of the BEs of O 1s (a) and $Al^{3+}$ 2p (b) during the $O_2$ oxidation at $p(O_2)$ = 0.2 Torr, with stepwise temperature increase from $T$ = 40 to 500 °C followed by vacuum annealing at 500 °C and then at 700 °C as shown in Figures 1 and 2.

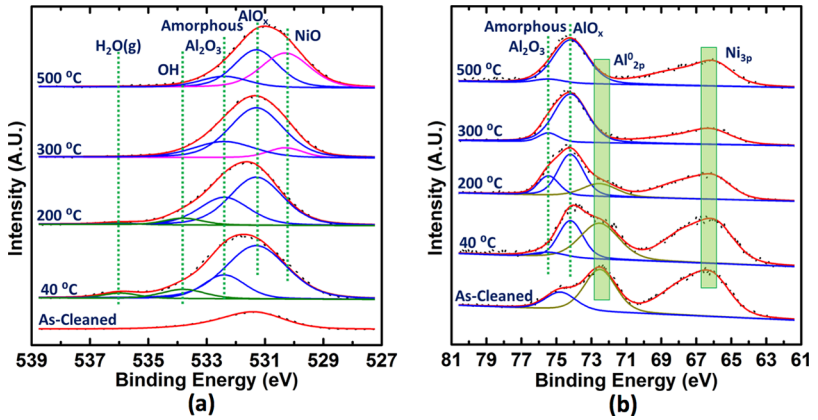


**Figure 4.** Photoemission spectra of the O 1s (a) and Al 2p−Ni 3p (b) regions of the NiAl(100) during the stepwise $H_2O$ oxidation at $p(H_2O)$ = 0.2 Torr and $T$ = 40, 200, 300, and 500 °C. The oxidation time is 25, 20, 30, and 40 min, respectively, at each $T$.

amorphous $Al_2O_3$ is crystallized to form $\gamma$-$Al_2O_3$. The BEs of the various O components are summarized in Table 2.

Identification of the different aluminum oxides from the O 1s spectra is also confirmed from the Al 2p spectra shown in Figure 1b. After the $O_2$ exposure at 40 °C, the $Al^{3+}$ 2p peak is deconvoluted into two components: one at BE = 74.4 eV, which can be attributed to $AlO_x$,[20,27] and the other at BE = 75.6 eV, which can be attributed to the amorphous $Al_2O_3$.[20,27] After the oxidation at 200 °C, the peak (BE = 74.4 eV) corresponding to $AlO_x$ completely disappears. The $Al^{3+}$ 2p peak is well fit by only one component at BE = 75.6 eV, which corresponds to the more stoichiometric amorphous $Al_2O_3$. When the temperature is increased to 300 °C and above, the $Al^{3+}$ 2p peak is well fit by two components, one at BE = 75.6 eV corresponding to the amorphous $Al_2O_3$ and the other at BE = 76.4 eV corresponding to $\gamma$-$Al_2O_3$.[25,30]

Both the O 1s and $Al^{3+}$ 2p peaks shift to higher BEs with further increase in the oxidation temperature to 300 °C and then to 500 °C. Such shifts to higher BEs at higher oxidation temperatures are further confirmed by the subsequent vacuum annealing of the as-oxidized sample. Figure 2a,b shows the spectra taken in vacuum at the corresponding annealing temperatures of the O 1s and Al 2p regions of the as-oxidized sample (right after the oxidation at 500 °C), which show that both the O 1s and $Al^{3+}$ 2p peaks shift only slightly after annealing at 500 °C for 30 min, as expected for aluminum oxide, because the oxide film is grown at 500 °C. However, the BEs have shifted by about 0.2−0.3 eV after further annealing at 750 °C for 30 min. This again confirms that the higher oxidation/annealing temperature results in the higher BEs of the O 1s and $Al^{3+}$ 2p peaks induced by the ordering of the amorphous oxide film. The shifts in the BEs of the O 1s and $Al^{3+}$ 2p peaks are summarized in Figure 3. Similarly, as shown in Figure 2, both the O 1s and $Al^{3+}$ 2p peaks can be deconvoluted into two peaks, one corresponding to amorphous $Al_2O_3$ having binding energies of 532.4 eV (O 1s) and 75.6 eV ($Al^{3+}$ 2p)[25,29,30] and the other corresponding to $\gamma$-$Al_2O_3$ with BEs of 533.3 eV (O 1s) and 76.4 eV ($Al^{3+}$ 2p).[25,29,30] The evolution of the relative intensities of the two peaks (Figure 2) shows that the amorphous $Al_2O_3$ is being gradually crystallized while annealing at the elevated temperatures. The shift in the BEs of the O 1s and $Al^{3+}$ 2p peaks can be attributed to the structure ordering (crystallization) in the aluminum oxide film as the temperature increases. The structural evolutions of the NiAl(100) surface and the aluminum oxide film were characterized using LEED and STM in our previous study, which showed that the aluminum oxide film formed at the relatively low temperatures (<300 °C) is amorphous and transforms to a crystalline state upon annealing above 450 °C.[10] It should be noted that the oxide film formed under oxygen pressure (0.2 Torr) is much thicker than the oxide films formed under the UHV oxidation conditions, which usually have a thickness of <5 Å.[13] The larger thickness of the oxide film may facilitate the formation of $\gamma$-$Al_2O_3$ as shown here, rather than the $\Theta$-$Al_2O_3$ phase by UHV annealing of ultrathin aluminum oxide films.[10,15,16] In general, the magnitude of the BE shift is



DOI: 10.1021/acs.langmuir.6b02752
Langmuir 2016, 32, 11414−11421

known to scale with the number of heterogeneous chemical bonds, and a larger BE shift can be attributed to a larger coordination number.[31] The BEs of the O 1s and $Al^{3+}$ 2p peaks of the amorphous aluminum oxide are reported to be about 0.5−1.0 eV lower than those of $\gamma$-$Al_2O_3$ on an Al substrate.[25,29,30] With the increase in the temperature, more crystalline oxide is developed by ordering the amorphous aluminum oxide, which results in the shifting of both O 1s and $Al^{3+}$ 2p peaks to the higher binding energies (Figure 3).

**3.2. Oxidation by Water Vapor.** The NiAl(100) surface cleaned similarly by sputtering and annealing in the AP-XPS chamber was oxidized by $H_2O$ under the same temperature and pressure conditions as $O_2$ oxidation. Figure 4a,b shows the evolution of the XPS spectra of the O 1s and Al 2p/Ni 3p regions acquired in situ during the oxidation. Compared with the freshly cleaned surface (Figure 1), it can be noted from Figure 4a,b that the as-cleaned NiAl(100) surface shows slightly more residual aluminum oxide, as indicated by the slightly stronger $Al^{3+}$ 2p peak because of the higher base pressure (~1 × $10^{-8}$ Torr) of the chamber. The oxide film reached its limiting thickness after $H_2O$ exposure at each $T$. There is no noticeable shift in the BEs of the metallic $Ni^0$ 3p and $Al^0$ 2p peaks with the temperature increase. However, the intensity of the metallic $Al^0$ 2p peak diminishes and disappears completely at 300 °C, whereas the metallic $Ni^0$ 3p peak is still visible (Figure 4b). The aluminum oxide film also shows stepwise increase in its thickness at lower temperatures and reaches about 15.7 Å after the $H_2O$ exposure at 200 °C, as shown in Table 3. The thickness of the aluminum oxide film cannot be estimated after the oxidation at 300 °C because the metallic $Al^0$ 2p peak is completely attenuated. However, the nonattenuation of the Ni 3p peak indicates that the diffusion of Ni from the substrate into the oxide film has occurred at a higher $T$. This is completely different from the $O_2$ exposure, for which both the metallic $Al^0$ 2p and $Ni^0$ 3p peaks are completely attenuated at 300 °C, as shown in Figure 1b. By contrast, the Ni 3p peak still shows a fair amount of intensity after the $H_2O$ exposure at 300 °C, and its relative intensity becomes even stronger from the subsequent $H_2O$ exposure at 500 °C.

**Table 3. Thicknesses of the Aluminum Oxide Films for the $O_2$ and $H_2O$ Oxidations of NiAl(100) and Subsequent Vacuum Annealing**

| temperature (°C) | 40 | 200 | 300 | 500 | 500 annealing | 750 annealing |
|---|---|---|---|---|---|---|
| $O_2$ (Å) | 10.8 | 16.3 | 22.0 | | | |
| $H_2O$ (Å) | 6.1 | 15.7 | | | | |

As shown in Figure 4a, the O 1s peak can be deconvoluted into three components with BE = 532.4, 531.3, and 533.8 eV for the $H_2O$ oxidation at 40 and 200 °C. As discussed in the $O_2$ oxidation section, the BEs of 532.4 and 531.3 eV are related to the amorphous $Al_2O_3$ and interfacial aluminum oxide $AlO_x$, respectively. The other peak with a higher BE of 533.8 eV is in good agreement with the reported values of OH species and is related to the O in the Al−OH bonds of aluminum hydroxide.[26,32,33] Also, the peak related to the gas phase of $H_2O$ is visible at a higher BE of 536 eV. However, the OH peak disappears at 300 °C and above, suggesting that aluminum hydroxide is not stable at the temperature above 300 °C and decomposes into aluminum oxide, consistent with the previous studies.[12,34] Meanwhile, using the BEs of the amorphous $Al_2O_3$ and $AlO_x$ peaks does not provide an overall good fitting to the O 1s spectra obtained at 300 and 500 °C, and a third peak at a lower BE of 530.3 eV arises. It is unlikely to form the $NiAl_2O_4$ spinel because the oxidation temperature employed here is far below the formation temperature of the $NiAl_2O_4$ spinel (~1100 °C in the form of a bulk spinel structure[35] and ~900 °C in the form of a thin film[36]). The absence of the $NiAl_2O_4$ phase can also be confirmed from the $Al^{3+}$ 2p peak, which has a higher BE in $NiAl_2O_4$ by ~1 eV than that in the $Al_2O_3$ peak. As shown in Figure 4b, no such BE shift is observed from the $Al^{3+}$ 2p peak. Therefore, the peak at BE = 530.3 eV is attributed to NiO. This conclusion is also based on the closeness of the O 1s BE of the component to the literature data for NiO.[27,37,38] The Ni 2p spectra were not collected to further confirm this conclusion because of the limitation of the beamline: the highest photon energy we can reach was around 700 eV, whereas the BE range for Ni 2p is from 840 to 880 eV. However, the O 1s peak at a lower BE and the existence of the Ni 3p peak at 300 °C and above provide clear evidence for NiO formation. As shown in Figure 4a, the relative intensity for the NiO component increases when the oxidation temperature increases from 300 to 500 °C, suggesting an enhanced NiO formation at higher temperatures. This trend is also proved by the relatively stronger intensity of the Ni 3p peak at 500 °C than that at 300 °C, as shown in Figure 4b.

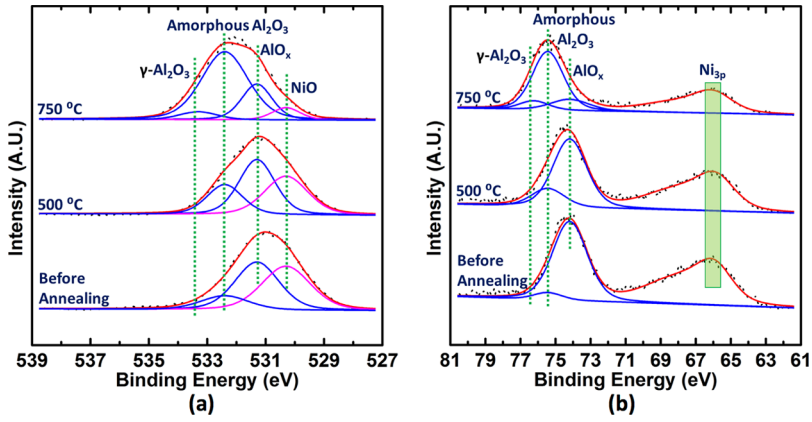


**Figure 5.** Photoemission spectra of the (a) O 1s and (b) Al 2p−Ni 3p regions of the NiAl(100) during the stepwise $H_2O$ oxidation at $p(H_2O)$ = 0.2 Torr and subsequent vacuum annealing at 500 °C and then 750 °C for 30 min each.



DOI: 10.1021/acs.langmuir.6b02752
Langmuir 2016, 32, 11414−11421

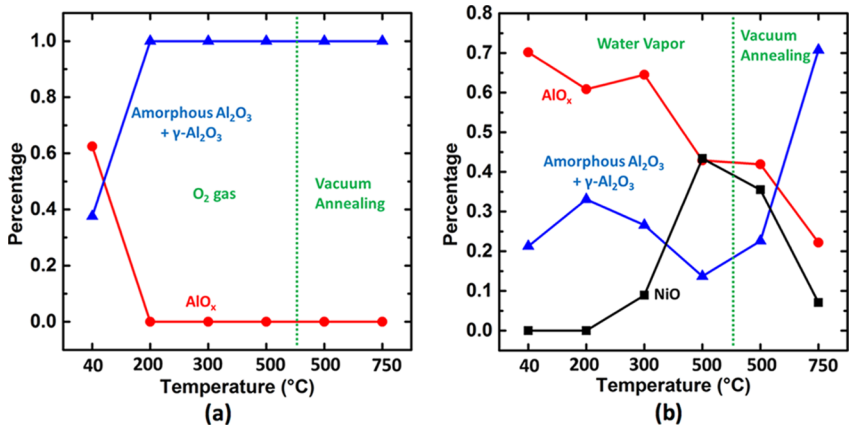


**Figure 6.** Temperature dependence of the composition of the oxide film: (a) $O_2$ oxidation and (b) $H_2O$ oxidation.

The effect of annealing temperature on the BEs of the different oxides is also confirmed by the subsequent vacuum annealing of the $H_2O$-formed oxide film. Both the O 1s and $Al^{3+}$ 2p peaks shift to high BEs (Figure 5). The O 1s spectra obtained from the as-oxidized sample (after the final $H_2O$ exposure at 500 °C) can be deconvoluted into three components at BE = 532.4, 531.3, and 530.3 eV, which correspond to $Al_2O_3$ (amorphous), $AlO_x$, and NiO, respectively. The O 1s spectra after the vacuum annealing at 500 °C are quite similar to those of the as-oxidized sample, except for the stronger peak intensity for the amorphous $Al_2O_3$ component. Figure 5a shows that a new small peak arises at a higher BE of 533.3 eV after vacuum annealing for 20 min at 750 °C. This peak corresponds to the formation of the crystallized $Al_2O_3$ ($\gamma$-$Al_2O_3$). It can be also seen from Figure 5a that the relative intensities of NiO and $AlO_x$ peaks decrease after the vacuum annealing at 500 °C and further decreases after the vacuum annealing at 750 °C. This indicates that the defective aluminum oxide ($AlO_x$) is gradually converted into the more stoichiometric $Al_2O_3$ upon annealing. The heat formation for $Al_2O_3$ (−1690.7 kJ/mol) is by a factor of seven larger than NiO (−240.8 kJ/mol).[39,40] The decrease in the relative intensity of the NiO peak at 500 and 750 °C shown in Figure 5a suggests that the NiO component is gradually reduced to Ni via the reaction NiO + Al → $Al_2O_3$ + Ni upon vacuum annealing, whereas the decrease in the relative intensity of the Ni 3p peak at 500 and 750 °C shown in Figure 5b is related to the dissolution of the reduced metallic Ni into the NiAl substrate. Becker et al. also reported a similar observation that the NiO formed on $Ni_3Al$ disappeared after annealing above 800 K.[41] The vacuum annealing-induced evolution of these oxide components derived from the O 1s spectra (Figure 5a) can be further confirmed from the $Al^{3+}$ 2p and Ni 3p peaks. As shown in Figure 5b, the $Al^{3+}$ peak associated with $\gamma$-$Al_2O_3$ shows up after annealing at 750 °C, whereas the relative intensity of the two peaks associated with the defective aluminum oxide ($AlO_x$) and NiO drops upon the vacuum annealing.

The composition of the oxide film can be calculated from the ratio of the relative intensity of the different oxide peaks with respect to the overall O 1s spectra. Figure 6 shows the evolution of the composition of the oxide films formed from the $O_2$ and $H_2O$ exposures and the subsequent vacuum annealing (for convenience of description, the composition of the stoichiometric $Al_2O_3$ is not further broken down into crystallized and noncrystallized ones). As shown in Figure 6a, the $O_2$-formed oxide film initially consists of both defective aluminum oxide ($AlO_x$) and stoichiometric aluminum oxide ($Al_2O_3$). The $AlO_x$ disappears completely at temperatures above 200 °C. By contrast, the $H_2O$-formed oxide film is dominated by the defective aluminum oxide ($AlO_x$) (Figure 6b), and the composition of the oxide film evolves from $(Al_2O_3)_{0.21}(AlO_x)_{0.7}(Al(OH)_3)_{0.09}$ at 40 °C to $(Al_2O_3)_{0.33}(AlO_x)_{0.61}(Al(OH)_3)_{0.06}$ at 200 °C. Noticeably, increasing the temperature to 300 °C results in the growth of NiO and the composition of the oxide film changes to $(Al_2O_3)_{0.27}(AlO_x)_{0.64}(NiO)_{0.09}$. NiO growth is further promoted after increasing the oxidation temperature to 500 °C, and the composition of the oxide film changes to $(Al_2O_3)_{0.14}(AlO_x)_{0.43}(NiO)_{0.43}$. Annealing the $H_2O$-formed oxide film promotes the formation of $Al_2O_3$ by consuming the defective $AlO_x$ and NiO, and the composition of the oxide film changes to $(Al_2O_3)_{0.23}(AlO_x)_{0.42}(NiO)_{0.35}$ after the vacuum annealing at 500 °C and then to $(Al_2O_3)_{0.71}(AlO_x)_{0.22}(NiO)_{0.07}$ after further annealing at 750 °C. The composition evolution of the oxide overlayer can be monitored in situ at an elevated temperature and pressure using AP-XPS as shown above. Such important information cannot be readily obtained with the use of a UHV-based XPS system (typically at pressures $<10^{-5}$ Torr) or exposure at high pressure in a separate chamber followed by transfer to UHV for analysis because the sample transfers can interrupt the reaction and induce oxide decomposition (e.g., NiO) or change the composition (e.g., $AlO_x$) of the oxide overlayer.

## 4. DISCUSSION

The detailed comparison of the oxidation of the NiAl(100) surface by $O_2$ and $H_2O$ made above illustrates that the $O_2$-formed oxide films have a more stoichiometric composition than the $H_2O$-formed oxide films under the same conditions of pressure and temperature. The different oxide film compositions have a direct consequence on the passivation properties of the oxide films. As shown in Figure 6, no NiO formation occurs for the $O_2$ exposure at any of the temperatures. By contrast, $H_2O$ exposure results in NiO growth at 300 °C, and further increasing the oxidation temperature leads to a significant NiO growth, for which the fraction of NiO in the oxide film increases from 9% at 300 °C to 43% at 500 °C.

The experimental results presented above reveal that the NiAl alloy exhibits selective oxidation during the $O_2$ oxidation, in which only Al participates in the oxide film formation (Figures 1 and 6). By contrast, the $H_2O$ oxidation at $T$ > 300


DOI: 10.1021/acs.langmuir.6b02752
Langmuir 2016, 32, 11414−11421

°C results in the simultaneous NiO growth (Figures 4 and 6). From a thermodynamic point of view, the formation of aluminum oxide is energetically strongly favored over the formation of NiO. The selective oxidation of Al in the NiAl alloy results in the enrichment of Ni in the oxide/substrate interface region, which has been observed for the oxidation of the NiAl(100) under UHV conditions.[12,13] In view of the much higher gas pressure in the present work, significant Ni enrichment can occur in the subsurface region because of the growth of the much thicker aluminum oxide film compared with the oxidation under the UHV conditions. As shown in Figures 1 and 4, the $O_2$-formed aluminum oxide film is dominated by stoichiometric $Al_2O_3$, which is more compact compared with the $H_2O$-formed oxide film that is dominated by the defective $AlO_x$. Therefore, the $O_2$-formed aluminum oxide film is a more effective barrier than the $H_2O$-formed oxide film in blocking the outward diffusion of Ni atoms from the subsurface region.

The equilibrium oxygen pressure for the selective oxidation of one component of an alloy depends on the alloy composition. The significant enrichment of Ni underneath the aluminum oxide layer lowers the equilibrium oxygen pressure for the Ni oxidation. Therefore, Ni can be driven to the outer surface through the existing aluminum oxide layer to form NiO, if allowed kinetically. As shown above, the $O_2$-formed oxide film is dominated by the stoichiometric $Al_2O_3$, for which the dense and compact atomic structure of the oxide film can provide better protection to the metallic substrate by barring the outward diffusion of the Ni atoms. Therefore, NiO formation is kinetically prohibited even at the elevated temperature of 500 °C, as shown in Figure 1. By contrast, the composition of the $H_2O$-formed oxide film is dominated by the defective $AlO_x$, for which the outward diffusion of Ni can be significantly promoted from the Ni-rich region underneath the aluminum oxide overlayer. As shown in Figure 6, a critical temperature of 300 °C is required to activate the outward diffusion of Ni through the defective $AlO_x$ layer. The outward diffusion of Ni is further promoted after increasing the oxidation temperature to 500 °C, which results in significantly more NiO growth (Figure 6).

## 5. CONCLUSIONS

A comparative study of the oxidation of NiAl(100) by molecular oxygen and water vapor at a near-ambient pressure (0.2 Torr) is performed using AP-XPS . $O_2$ exposure leads to the selective oxidation of Al at temperatures ranging from 40 to 500 °C. By contrast, $H_2O$ exposure results in the selective oxidation of Al at 40 and 200 °C; increasing the oxidation temperature above 300 °C leads to simultaneous NiO formation. Based on the detailed analyses of the BE shifts and the evolution of the relative intensities of the O 1s, $Al^{3+}$ 2p, and Ni 3p peaks, we show that the oxide film formed from the $O_2$ oxidation has a stoichiometric $Al_2O_3$ structure that provides improved protection to the metallic substrate by barring the outward diffusion of Ni. By contrast, the aluminum oxide film formed by the $H_2O$ oxidation has a defective (and thus less protective) structure that allows outward diffusion of Ni for simultaneous NiO formation. These results demonstrate that the passivation properties of an oxide film depend on the type of the oxidizing species used for the surface passivation.

## AUTHOR INFORMATION

### Corresponding Author

*E-mail: gzhou@binghamton.edu.

### Notes

The authors declare no competing financial interest.

## ACKNOWLEDGMENTS

This work was supported by the U.S. Department of Energy, Office of Basic Energy Sciences, Division of Materials Sciences and Engineering under Award No. DE-SC0001135. The research was carried out in part at the Center for Functional Nanomaterials and the National Synchrotron Light Source, which are supported by the U.S. Department of Energy, Office of Basic Energy Sciences, under Contract No. DE-SC0012704.

## REFERENCES

(1) Lin, W.-C.; Kuo, C.-C.; Luo, M.-F.; Song, K.-J.; Lin, M.-T. Self-aligned Co nanoparticle chains supported by single-crystalline $Al_2O_3$/NiAl(100) template. *Appl. Phys. Lett.* **2005**, *86*, 043105.

(2) Luo, M. F.; Chiang, C. I.; Shiu, H. W.; Sartale, S. D.; Kuo, C. C. Patterning Co nanoclusters on thin-film $Al_2O_3$/NiAl(100). *Nanotechnology* **2005**, *17*, 360.

(3) Sartale, S. D.; Shiu, H. W.; Ten, M. H.; Huang, J. Y.; Luo, M. F. Scanning tunneling microscopy study of growth of Pt nanoclusters on thin film $Al_2O_3$/NiAl(100). *Surf. Sci.* **2006**, *600*, 4978−4985.

(4) Luo, M. F.; Shiu, H. W.; Ten, M. H.; Sartale, S. D.; Chiang, C. I.; Lin, Y. C.; Hsu, Y. J. Growth and electronic properties of Au nanoclusters on thin-film $Al_2O_3$/NiAl(100) studied by scanning tunnelling microscopy and photoelectron spectroscopy with synchrotron radiation. *Surf. Sci.* **2008**, *602*, 241−248.

(5) Méndez, J.; Niehus, H. Growth of chromium on the structured surface of $Al_2O_3$/NiAl(100). *Appl. Surf. Sci.* **1999**, *142*, 152−158.

(6) Gaßmann, P.; Franchy, R.; Ibach, H. Preparation of a well ordered aluminum oxide layer on NiAl(001). *J. Electron Spectrosc. Relat. Phenom.* **1993**, *64*, 315−320.

(7) Gassmann, P.; Franchy, R.; Ibach, H. Investigations on phase transitions within thin $Al_2O_3$ layers on NiAl(001)—HREELS on aluminum oxide films. *Surf. Sci.* **1994**, *319*, 95−109.

(8) Blum, R.-P.; Ahlbehrendt, D.; Niehus, H. Growth of $Al_2O_3$ stripes in NiA(001). *Surf. Sci.* **1998**, *396*, 176−188.

(9) Qin, H.; Zhou, G. The formation of double-row oxide stripes during the initial oxidation of NiAl(100). *J. Appl. Phys.* **2013**, *114*, 083513.

(10) Qin, H.; Sutter, P.; Zhou, G. The Crystallization of Amorphous Aluminum Oxide Thin Films Grown on NiAl(100). *J. Am. Ceram. Soc.* **2014**, *97*, 2762−2769.

(11) Frémy, N.; Maurice, V.; Marcus, P. X-ray photoelectron spectroscopy study of thin oxide layers formed on (001)-oriented $\beta$-NiAl single-crystal surfaces. *Surf. Interface Anal.* **2002**, *34*, 519−523.

(12) Cai, N.; Liu, Q.; Tong, X.; Zhou, G. X-ray Photoelectron Spectroscopy Study of the Passivation of NiAl(100) by Water Vapor. *Langmuir* **2014**, *30*, 774−783.

(13) Cai, N.; Qin, H.; Tong, X.; Zhou, G. Growth of ultrathin amorphous alumina films during the oxidation of NiAl(100). *Surf. Sci.* **2013**, *618*, 20−26.

(14) Blum, R.-P.; Niehus, H. Initial growth of $Al_2O_3$ on NiAl(001). *Appl. Phys. A: Mater. Sci. Process.* **1998**, *66*, S529−S533.

(15) Frémy, N.; Maurice, V.; Marcus, P. Initial Stages of Growth of Alumina on NiAl(001) at 1025 K. *J. Am. Ceram. Soc.* **2003**, *86*, 669−675.

(16) Qin, H.; Chen, X.; Li, L.; Sutter, P. W.; Zhou, G. Oxidation-driven surface dynamics on NiAl(100). *Proc. Natl. Acad. Sci. U.S.A.* **2015**, *112*, E103−E109.

(17) Toyoshima, R.; Shimura, M.; Yoshida, M.; Monya, Y.; Suzuki, K.; Amemiya, K.; Mase, K.; Mun, B. S.; Kondoh, H. A near-ambient-pressure XPS study on catalytic CO oxidation reaction over a Ru(10$\bar{1}$0) surface. *Surf. Sci.* **2014**, *621*, 128−132.



DOI: 10.1021/acs.langmuir.6b02752
*Langmuir* 2016, 32, 11414−11421

(18) Eren, B.; Heine, C.; Bluhm, H.; Somorjai, G. A.; Salmeron, M. Catalyst Chemical State during CO Oxidation Reaction on Cu(111) Studied with Ambient-Pressure X-ray Photoelectron Spectroscopy and Near Edge X-ray Adsorption Fine Structure Spectroscopy. *J. Am. Chem. Soc.* **2015**, *137*, 11186−11190.
(19) Lee, H. C.; Kim, B. M.; Jeong, C. K.; Toyoshima, R.; Kondoh, H.; Shimada, T.; Mase, K.; Mao, B.; Liu, Z.; Lee, H.; Huang, C.-Q.; Li, W. X.; Ross, P. N.; Mun, B. S. Surface segregation and oxidation of $Pt_3Ni(111)$ alloys under oxygen environment. *Catal. Today* **2016**, *260*, 3−7.
(20) Shavorskiy, A.; Müller, K.; Newberg, J. T.; Starr, D. E.; Bluhm, H. Hydroxylation of Ultrathin $Al_2O_3$/NiAl(110) Films at Environmental Humidity. *J. Phys. Chem. C* **2014**, *118*, 29340−29349.
(21) Starr, D. E.; Liu, Z.; Hävecker, M.; Knop-Gericke, A.; Bluhm, H. Investigation of solid/vapor interfaces using ambient pressure X-ray photoelectron spectroscopy. *Chem. Soc. Rev.* **2013**, *42*, 5833−5857.
(22) Maurice, V.; Frémy, N.; Marcus, P. Hydroxylation-induced modifications of the $Al_2O_3$/NiAl(001) surface at low water vapour pressure. *Surf. Sci.* **2005**, *581*, 88−104.
(23) Marcus, P.; Hinnen, C.; Olefjord, I. Determination of attenuation lengths of photoelectrons in aluminium and aluminium oxide by angle-dependent X-ray photoelectron spectroscopy. *Surf. Interface Anal.* **1993**, *20*, 923−929.
(24) Delgass, W. N.; Hall, G. L.; Kellerman, R.; Lunsford, J. H. *Spectroscopy in Heterogeneous Catalysis*; Academic press: New York, 1979.
(25) Jeurgens, L. P. H.; Sloof, W. G.; Tichelaar, F. D.; Mittemeijer, E. J. Composition and chemical state of the ions of aluminium-oxide films formed by thermal oxidation of aluminium. *Surf. Sci.* **2002**, *506*, 313−332.
(26) Chen, C.; Splinter, S. J.; Do, T.; McIntyre, N. S. Measurement of oxide film growth on Mg and Al surfaces over extended periods using XPS. *Surf. Sci.* **1997**, *382*, L652−L657.
(27) Garza, M.; Magtoto, N. P.; Kelber, J. A. Characterization of oxidized $Ni_3Al(110)$ and interaction of the oxide film with water vapor. *Surf. Sci.* **2002**, *519*, 259−268.
(28) Cai, N.; Zhou, G.; Müller, K.; Starr, D. E. Tuning the Limiting Thickness of a Thin Oxide Layer on Al(111) with Oxygen Gas Pressure. *Phys. Rev. Lett.* **2011**, *107*, 035502.
(29) Venezia, A. M.; Loxton, C. M. Low pressure oxidation of $Ni_3Al$ alloys at elevated temperatures as studied by X-ray photoelectron spectroscopy and Auger spectroscopy. *Surf. Sci.* **1988**, *194*, 136−148.
(30) Bianconi, A.; Bachrach, R. Z.; Hagstrom, S. B. M.; Flodström, S. A. Al-$Al_2O_3$ interface study using surface soft-x-ray absorption and photoemission spectroscopy. *Phys. Rev. B: Condens. Matter Mater. Phys.* **1979**, *19*, 2837−2843.
(31) Graupner, H.; Hammer, L.; Heinz, K.; Zehner, D. M. Oxidation of low-index FeAl surfaces. *Surf. Sci.* **1997**, *380*, 335−351.
(32) Niu, C.; Shepherd, K.; Martini, D.; Tong, J.; Kelber, J. A.; Jennison, D. R.; Bogicevic, A. Cu interactions with $\alpha$-$Al_2O_3(0001)$: Effects of surface hydroxyl groups versus dehydroxylation by Ar-ion sputtering. *Surf. Sci.* **2000**, *465*, 163−176.
(33) Cai, N.; Zhou, G.; Müller, K.; Starr, D. E. Comparative Study of the Passivation of Al(111) by Molecular Oxygen and Water Vapor. *J. Phys. Chem. C* **2013**, *117*, 172−178.
(34) Digne, M.; Sautet, P.; Raybaud, P.; Toulhoat, H.; Artacho, E. Structure and Stability of Aluminum Hydroxides: A Theoretical Study. *J. Phys. Chem. B* **2002**, *106*, 5155−5162.
(35) Calow, C. A.; Porter, I. T. The solid state bonding of nickel to alumina. *J. Mater. Sci.* **1971**, *6*, 156−163.
(36) Loginova, E.; Cosandey, F.; Madey, T. E. Nanoscopic nickel aluminate spinel ($NiAl_2O_4$) formation during NiAl(111) oxidation. *Surf. Sci.* **2007**, *601*, L11−L14.
(37) Cappus, D.; Xu, C.; Ehrlich, D.; Dillmann, B.; Ventrice, C. A.; Al Shamery, K.; Kuhlenbeck, H.; Freund, H.-J. Hydroxyl groups on oxide surfaces: NiO(100), NiO(111) and Cr2O3(111). *Chem. Phys.* **1993**, *177*, 533−546.
(38) Tyuliev, G. T.; Kostov, K. L. XPS/HREELS study of NiO films grown on Ni(111). *Phys. Rev. B: Condens. Matter Mater. Phys.* **1999**, *60*, 2900−2907.
(39) Sobczak, N.; Oblakowski, J.; Nowak, R.; Kudyba, A.; Radziwill, W. Interaction between liquid aluminum and NiO single crystals. *J. Mater. Sci.* **2005**, *40*, 2313−2318.
(40) Wen, J. Z.; Ringuette, S.; Bohlouli-Zanjani, G.; Hu, A.; Nguyen, N. H.; Persic, J.; Petre, C. F.; Zhou, Y. N. Characterization of thermochemical properties of Al nanoparticle and NiO nanowire composites. *Nanoscale Res. Lett.* **2013**, *8*, 1−9.
(41) Becker, C.; Kandler, J.; Raaf, H.; Linke, R.; Pelster, T.; Dräger, M.; Tanemura, M.; Wandelt, K. Oxygen adsorption and oxide formation on $Ni_3Al$ (111). *J. Vac. Sci. Technol., A* **1998**, *16*, 1000−1005.



DOI: 10.1021/acs.langmuir.6b02752
*Langmuir* 2016, 32, 11414−11421